IEEE Photonics Journal
An IEEE Photonics Society Publication

Open Access

Polarization Guided Autoregressive Model for Depth Recovery

Volume 9, Number 3, June 2017

Mohamed Reda
Yongqiang Zhao
Jonathan Cheung-Wai Chan

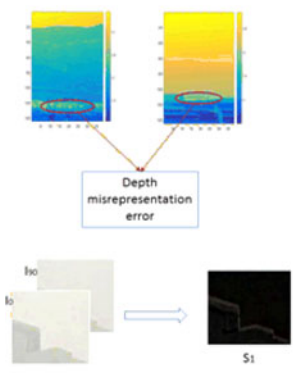

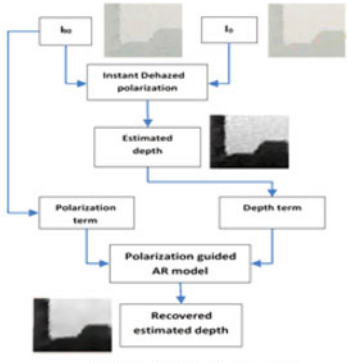

Flowchart of our proposed method

DOI: 10.1109/JPHOT.2017.2706748
1943-0655 © 2017 IEEE

IEEE photonics SOCIETY

IEEE

Polarization Guided Autoregressive Model for Depth Recovery

Mohamed Reda,[1] Yongqiang Zhao,[1] and Jonathan Cheung-Wai Chan[2]

[1]School of Automation, Northwestern Polytechnical University, Xi'an 710072, China
[2]Department of Electronics and Informatics, Vrije Universiteit Brussel, Brussels 1050, Belgium

DOI:10.1109/JPHOT.2017.2706748

Manuscript received April 20, 2017; revised May 15, 2017; accepted May 16, 2017. Date of publication May 23, 2017; date of current version June 2, 2017. This work was supported in part by the National Natural Science Foundation of China under Grant 61371152, in part by the National Natural Science Foundation of China and South Korean National Research Foundation Joint Funded Cooperation Program under Grant 61511140292, and in part by the Fundamental Research Funds for the Central Universities under Grant 3102015ZY045. Corresponding author: Mohamed Reda (e-mail: arabian_hero@hotmail.com).

Abstract: The Instant Dehaze method used polarized images to obtain a dehazed image and an estimated depth map of the scene. Haze due to atmospheric absorption and scattering causes degradation in image quality and the estimated depth. This estimated depth is misrepresented due to high degree of polarization and scene's objects directly illuminated by the sun. In this paper, a polarization guided autoregressive (AR) model for depth recovery is presented. This proposed method restores the estimated depth map by incorporating polarized data to an adaptive AR model. First a 90° polarized image is used in our polarization term of AR coefficient, then the Stokes vector component S_1 is used in our polarization guided depth map in the depth term of AR coefficient. The experimental results show that our method outperforms existing state-of-the-art schemes and improves conventional polarization dehazing method.

Index Terms: Imaging, scattering, visualization, optical and other.

1. Introduction

Outdoor scenes are usually affected by haze, fog, and smoke due to atmospheric absorption and scattering, which degraded image quality and the estimated depth map. Recently there are heightening interests in enhancement of images affected by weather phenomena. The main target is the enhancement of images taken in environment with poor visibility [1]–[4]. Information of the scenes such as depth map can be obtained because of atmospheric scattering [5]–[9]. Some of the enhancement methods applied in this field require prior information about the scene such as the distance between objects [2]. Other methods depend on radiation sources and detection devices [10], [11].

The depth map consists of the depth information of real scenes, which plays an important role for many applications such as 3D reconstruction, augmented reality, and navigation applications. This real depth map is difficult to be obtained because we do not know the real distance of the scene. There are two main categories of methods to estimate the depth map: the passive methods and the active methods. The passive methods compute the depth information from two-view or multi-view images through triangulation and correspondence matching. But these methods still

have some inherent problems. As accurate image registration is a pre-requisite for such approach, inefficiency is observed for textureless areas [12]. While the active methods acquire depth information by devices such as Time-of-flight (ToF) camera and Kinect. The laser range scanner techniques [13] achieve high accuracy but have long processing time and they are inconvenient for dynamic scenes. ToF cameras [14] have the advantage of capturing the dynamic scenes in real time, but the captured images are unavoidably noisy and have lower resolutions compared with conventual color cameras. The generated depth maps from the Kinect have some holes. It is also sensitive to environmental condition such as sunlight and it is not suitable for outdoor applications [15].

As mentioned above, conventional methods for obtaining the estimated depth map have their disadvantages. Haze effects make this problem more sever as it causes a degradation in the image quality and subsequently hampers the estimation of depth. Our target is to obtain accurate depth information from a dehazed depth map.

The Instant Dehazing method described in [16], [17] is based on the analysis of polarized images captured by a polarizer [18], [19]. The output is a dehazed image, and the estimated depth map. This approach relies on the fact that atmospheric particles are partially polarized [20], [21]. However, a polarization filter alone cannot remove the haze, that is why further analysis of polarized images is needed [22], [23]. This Instant Dehazing approach does not need a model for the mechanism of scattering. The principle is to obtain two components - the airlight and the scene radiance in the haze free environment - by using two perpendicular polarized images [24], [25]. As a by-product, an estimated depth map is obtained. This estimated depth map is not accurate and its stability will decrease as the degree of polarization decreases. Also, for conditions like very dense haze and overcast sky, it is less effective.

The main point of interest in this paper is the estimated depth map after dehazing. To overcome limitations of the estimated depth map, many research works proposed techniques for depth recovery. Usually, enhancement is achieved with a joint image filtering technique using a low-resolution depth map and a high-resolution color image [14], [26]–[28]. The adaptive color-guided AR model (ADAR) [29], [30] has been used to obtain a unified depth recovery framework for both ToF and Kinect depth cameras. It creates a pixel-wise adaptive AR predictor. By minimizing the AR prediction errors subjecting to the observation consistency, the missing depth information of the depth map is recovered. All these methods are targeting normal images, not polarized images.

In this paper, we propose a method to recover the estimated depth based on AR model by using polarized images. A 90-degree polarization (I_{90}) is used to replace the color image in the color term of the AR coefficient [29], [30], then we will call this term the polarization term. Our contribution is the polarization guided depth map obtained by applying the Stokes vector component S_1 to the estimated depth guided map [31], then applying it to the depth term of the AR coefficient. The Stokes vector component S_1 is the difference between the intensities of two polarized images at zero degree (I_0) and ninety degree (I_{90}), gives us the information about the surface of objects and their edges in the scene. In addition, S_1 has the Gaussian characteristics that make smoothing effect for reduce the noise and to ensure robust edge detection [32]. It is known that edges are visually important for image perception, so restoring the sharpness of edges has a major effect on image quality. S_1 will enhance the sharpness of the edges and will increase the depth values in dehazed images. This will lead to an increase of the depth term and hence the AR coefficient. As the AR coefficient increases, the depth map will be enhanced and become more accurate.

The experiments results demonstrate that our proposed method achieves the best quality when compared with the state-of-the-art schemes. The remainder of this paper is organized as follows. First, the theoretical background is introduced in Section 2, including Instant Dehazing using polarization and depth recovery using the adaptive auto-regressive model. Then, we discuss our proposed method in Section 3. In Section 4, we describe the data preparation and the experiments followed by results and their comparison with the dark channel method and the ADAR model. Finally, the conclusion presented in Section 5

2. Theoretical Background

2.1 Instant Dehazing of Images Using Polarization

The airlight is considered as one of the sources of image degradation accompanied with atmospheric scattering. In this process, light coming from the illumination sources (e.g., the sun) is scattered towards the viewer The airlight A increases with the distance z from the object [5], [16], [17]:

$$A = A_\infty(1 - e^{-\beta z}) \tag{1}$$

where β is the scattering coefficient and A_∞ is the airlight corresponding to an object at an infinite distance (horizon).

Atmospheric scattering also degrades images by attenuating the light emanating from scene objects. The light energy that reaches the viewer is called the direct transmission T which is a function of the distance and scattering coefficient β and is given by:

$$T = e^{-\beta z} \tag{2}$$

The measured overall intensity I^{total} is the incoherent sum of the airlight A and the direct transmission T [16], [17]:

$$I^{total} = A + T \tag{3}$$

which is also equal to the sum of I_0 and I_{90}

$$I^{total} = I_0 + I_{90} \tag{4}$$

According to the algorithm in [16], the scene radiance in free atmospheric scattering environment is estimated and the dehazed image ($\hat{R}$) is given by:

$$\hat{R} = \frac{\hat{I}^{total} - \hat{A}}{\hat{e}^{-\beta z}} \tag{5}$$

As a by-product of the dehazing process, the estimated depth map is obtained by:

$$\hat{\beta} z(x,\ y) = -\log[1 - \hat{A}(x,\ y)/A_\infty] \tag{6}$$

then we combine the depth map for each color channel: r, g and b by averaging:

$$\overline{\beta z} = \left[\hat{\beta}_r z(x,\ y) + \hat{\beta}_g z(x,\ y) + \hat{\beta}_b z(x,\ y)\right]/3 \tag{7}$$

We will use this estimated depth $\overline{\beta z}$ in our proposed. However, this estimated depth map has some problems. The degree of polarization of the hazy distant objects is small relative to the airlight. On the other hand, this may be not true for some closer objects. that are directly illuminated by the sun. Because a significant partial polarization was observed and that makes those closer objects appear to be distant objects.

In Fig. 1, the orange highlighted by the red circle corresponded wrongly as distant objects due to high degree of polarization and sun illumination. The Instant Dehaze method is based on partial polarization of airlight. Its stability will decrease as the degree of polarization decreases. Also, it may be ineffective under an overcast sky, or in situations of fog or very dense haze.

2.2 Auto-Regressive Model and Depth Recovery

Any captured depth map is considered as a degraded version of the ground truth. The degradation model of a captured depth map [29], [30] is given by:

$$d^0 = Hd + n \tag{8}$$

where d and d^0 denote the vector form of the underlying perfect depth map and the captured depth map respectively, H represents the observation matrix and n is additive noise.

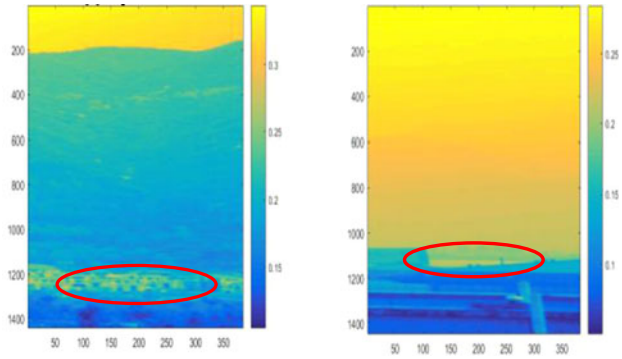

(a) (b)

Fig. 1. (a) and (b) represents the estimated depth map of the scene. The farther the object the higher is the value of colormap. The red circles highlight the misrepresentation errors.

The AR model has been used in many image processing applications. The key of the AR model is that a signal can be regenerated by the signal itself. The predicted depth map $\tilde{D}_x$ by the AR model from the depth map D is given by:

$$\tilde{D}_x == \sum_{y \in N_x} a_{x,y} D_y \tag{9}$$

Where $\tilde{D}_x$ is the predicted depth map at location x, D_y is the depth value at location y, $N(x)$ is the neighborhood of pixel x, $a_{x,y}$ denotes the AR coefficient for pixel y in the neighborhood $N(x)$.

The combination of the depth and the color information have strong correlation in terms of geometrical structures [33]. Depth maps have low resolution and low signal-to-noise ratio while color images are characterized by high resolution and high quality. Designing the AR predictors is done by using the captured depth map and the accompanied color image and this is known as the color guided AR model.

The AR coefficient $a_{x,y}$ of a color guided AR model consists of two terms, the depth term and color term and is given by:

$$a_{x,y} = \frac{1}{S_x} a^{\hat{D}}_{x,y} a^{I}_{x,y} \tag{10}$$

where S_x is the normalization factor, $a^{\hat{D}}_{x,y}$ and $a^{I}_{x,y}$ are the depth term and color term, respectively.

The adaptive color-guided AR (ADAR) model is a bilateral-weighted non-local mean (NLM) filter [34]–[36] has a shape-based adaptive neighborhood instead of patch-based, also exploits more correlations for pixels around discontinuities.

3. Proposed Method

Our proposed method is based on the polarization information and the AR model in [29], [30]. Related studies have shown that using polarized images is useful in providing us with the polarization information of the scene, which is essential for image processing applications such as object recognition [37], [38], scene segmentation [39] and material classification [40], [41].

Polarization of the light provides a way to characterize physical properties of objects of different materials. The polarization components of electromagnetic wave have the relationship that parallel component is greater than the perpendicular component, which is reflected as a 90° difference of the phase angle between the surface of specular reflection and diffuse reflection in the polarization angle images. According to this difference, we can detect the edge of the surface of specular reflection and diffuse reflection [42]. Polarization gives a great benefit to improve precision of edge detection [43], [44].

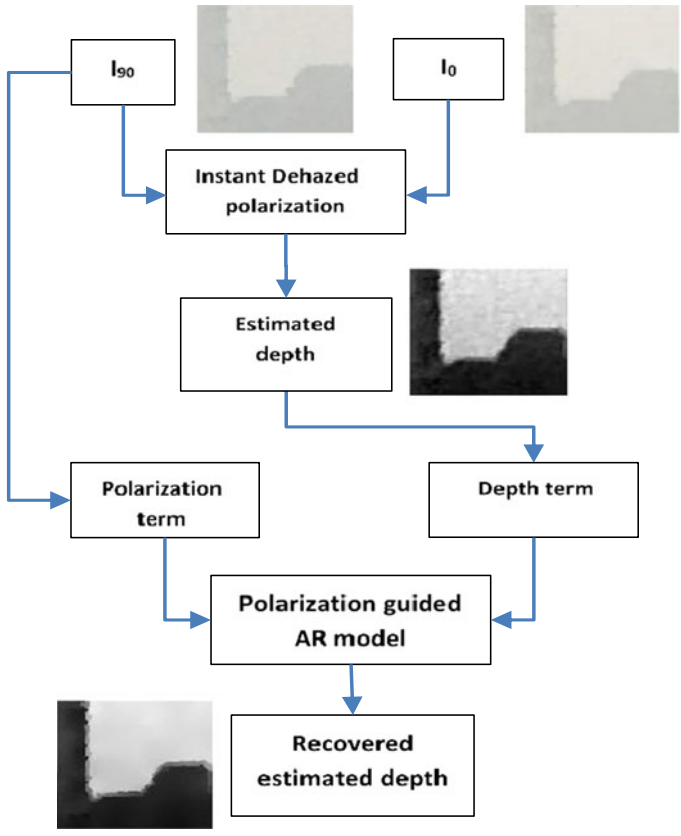

Fig. 2. Flowchart of our proposed method.

The flow chart of our proposed method is shown in Fig. 2. Our contribution is how to use the polarization information in the recovery of the depth map. Starting from applying the Instant Dehazing method on the two-perpendicular polarized images to get the dehazed image and the estimated depth map. Then, calculating the Stokes vector component S_1, which will be used in improving the edge information and will subsequently enhance the values of the depth map. S_1 will also overcome the problem of conventional dehaze methods by its Gaussian characteristics that has smoothing effect. Then, applying the 90-degree polarized image and our polarization guided depth map D_{0new} to the AR model. Finally, we obtain our recovered depth from our proposed method.

The Stokes vector is considered as a common representation of a polarization state [45], [46]. A 2×1 column vector formed from the two perpendicular polarized images is assembled over a scene with x-y spatial coordinates as shown in this equation:

$$\begin{pmatrix} S_0(x,y) \\ S_1(x,y) \end{pmatrix} = \begin{pmatrix} I(x,y,0^\circ) + I(x,y,90^\circ) \\ I(x,y,0^\circ) - I(x,y,90^\circ) \end{pmatrix} \tag{11}$$

where S_0 represents the total intensity of the remitted and collected light, S_1 represents the difference in intensities between the horizontal and vertical linearly polarized components. The intensity value of I_0 is greater than I_{90}, especially near the edges of the objects due to the specular reflection and the diffuse reflection. The difference between the intensity value of I_0 and I_{90} for the same pixel will show the edge information of the scene's objects.

In order to show the effectiveness of S_1, we provide several examples in Fig. 3. The output of S_1 shows how it makes the edges appear obviously and sharp relative to the scene contents. The outputs of S_1 as shown in Fig. 3(b) validate its efficiency in obtaining the edge information in scenes with different environmental conditions. Since the output of S_0 is the summation of the two

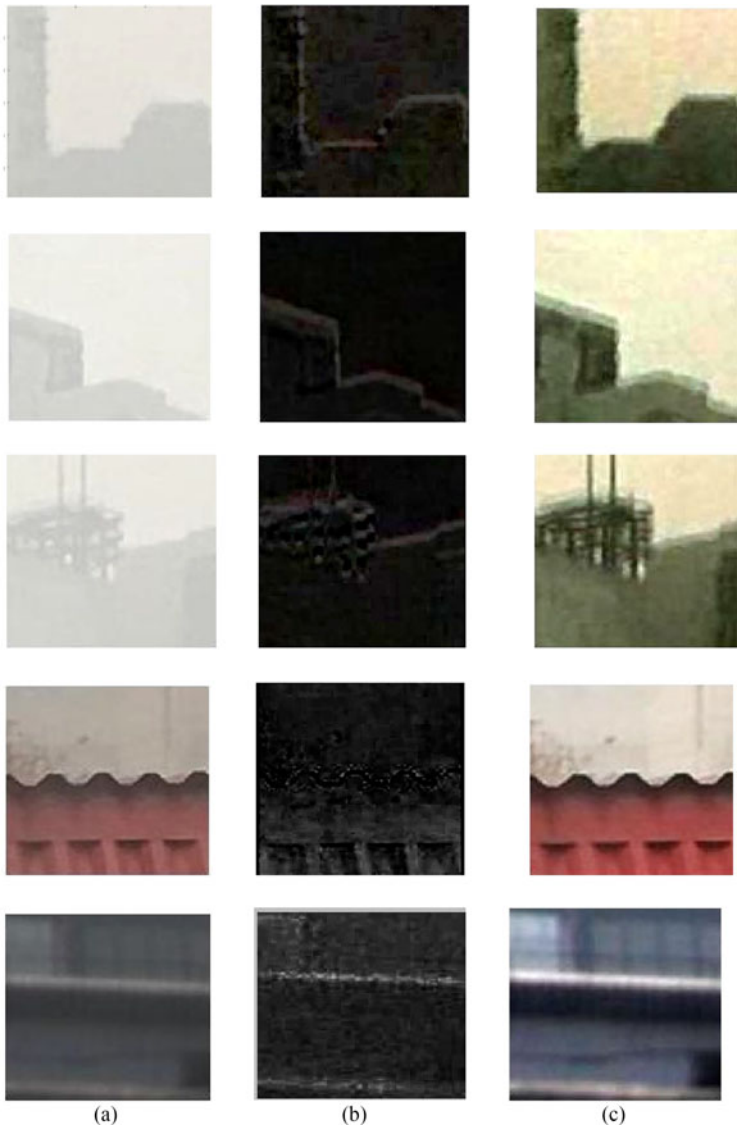

Fig. 3. The first column (a) is an example of polarized images I_0 in different environmental scene conditions, the second column (b) is the output of S_1, and the third column (c) is the output of S_0 after normalization. (a) I_0 (b) S_1 (c) S_0.

perpendicular polarized images I_0 and I_{90}. We normalize it to be in range of 0 to 255. The output of normalized S_0 shown in Fig. 3(c) increase the contrast of the scene. After comparing the output of S_1 with the output of S_0, we choose S_1 to give the edge information for our proposed method. In addition, we will also compare the histograms for both of S_1 and S_0 as shown in Fig. 4.

In our proposed method, we will use the Stokes vector component S_1. Where, S_1 is the difference between the intensity value of the two perpendicular polarized images I_0 and I_{90}. The intensity value of I_0 is greater than I_{90}, especially near the edges of the objects due to the specular reflection and the diffuse reflection depending on the structure of the surface. The intensity value computed from the difference between I_0 and I_{90} for the same pixel will show the edge information of the scene's objects as shown in Fig. 3(b). This information will enhance the recovered depth.

The histograms of S_0 shown in Fig. 4(c) represent pixels value spread over a large range of intensity values due to the summation of I_0 and I_{90}. On the contrary, the histograms of S_1 shown in Fig. 4(b) is concentrated and has gradient values instead of discrete binary values. The histograms

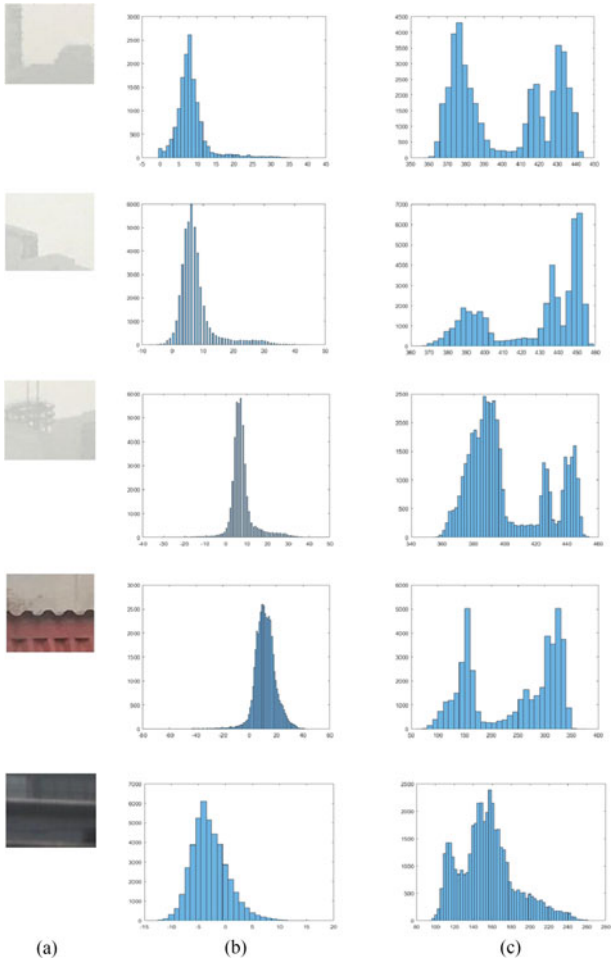

Fig. 4. The first column (a) is an example of polarized images I_0, the second column (b) is the histograms of S_1 which has Gaussian characteristics that make smoothing effect for suppressing the noise, and the third column (c) is the histograms of S_0. (a) I_0 (b) S_1 (c) S_0.

of different scenes validate statistically that S_1 has approximately Gaussian characteristics. The Gaussian characteristics is used in smoothing images. Smoothing has a positive effect to reduce noise and to ensure robust of our model, especially in overcoming the misrepresentation problems of the estimated depth of the Instant Dehaze method [32].

We propose the polarization guided depth map D_{0new} (our contribution) by applying the Stokes vector component S_1 to the estimated depth guided map D_0, which is given by:

$$D_{0new} = D_0 S_1 \ = D_0 (I_0 - I_{90}) \tag{12}$$

The output D_{0new} is shown in Fig. 5, which shows the effect of S_1 on the depth value

The restoration of the depth map will be performed by applying the proposed depth guided map D_{0new} to the depth term ($a^{\hat{D}}_{x,\,y}$) of the AR coefficient based on the adaptive AR model in [29], [30]. In this way, we will get the advantage of the polarization information in the depth recovery. Our depth term ($a^{\hat{D}}_{x,y}$) will be defined on the initial estimated depth map ($\hat{D}_{new}$) by a range filter and is given by:

$$a^{\hat{D}}_{x,y} = \exp\left(-\frac{(\hat{D}_{newx} - \hat{D}_{newy})^2}{\sigma_1^2}\right) \tag{13}$$

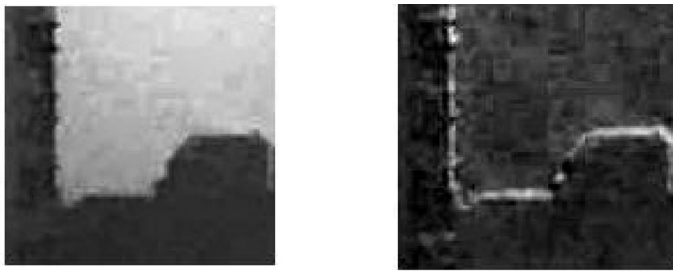

(a) (b)

Fig. 5. The depth map (a) D_0 and (b) D_{0new} after applying S_1 and its effect on the depth value.

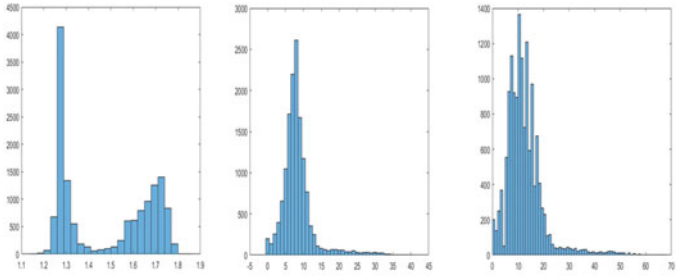

(a) (b) (c)

Fig. 6. The histogram of the (a) D_0, (b) S_1 and (c) polarization guided depth map D_{0new}.

where σ_1 is the decay rate of the range filter and its value will increase when $\hat{D}_{newx}$ is close to $\hat{D}_{newx}$ and the depth term is used to avoid the incorrect depth prediction.

We notice from Fig. 6, which illustrates the histograms of D_0, S_1, and the effect of S_1 on the D_{0new}, that the depth value of D_{0new} is higher than that of D_0 and the distribution of the values are more concentrated and having Gaussian shape. Increasing the depth value will increase the depth term of the AR coefficient and hence the AR coefficient will increase too. The AR coefficient should be large enough to have sufficient information for predicting the depth map.

Also, by applying the polarized image instead of the color image in AR coefficient, our polarization term is given by:

$$a^{l}_{x,y} = exp\left(-\frac{\sum_{i\in C}\left\|B_x \circ \left(P^i_x - P^i_y\right)\right\|^2_2}{2\times 3\times \sigma_2^2}\right) \tag{14}$$

where σ_2 controls the decay rate of the exponential function, P^i_x denotes an operator that extracts a $W \times W$ patch centered at x in a color channel i of the I_{90} polarized image, $\circ$ represents the element-wise multiplication. The bilateral filter kernel B_x is defined in the extracted $W \times W$ patch.

By applying the AR coefficient $a_{x,y}$ as mentioned in (13) and (14) based on the AR model [33]–[35], the estimated depth map is recovered. The recovered depth is quadratic with respect to the depth map value. So, it can be reformulated as an unconstrained quadratic equation and then analyzed as linear systems. The model is equivalent to the following minimization operation with respect to the recovered depth map d:

$$\min_d \left\|d^P - Pd\right\|^2_2 + \lambda \left\|d - Qd\right\|^2_2 \tag{15}$$

where d^P is the vector form estimated depth guided map D_0, P is the observation matrix that represent the sampling identity matrix and Q is the prediction matrix corresponding to AR predictors $a_{x,y}$. Where the first term is the data term and the second term is the AR term.

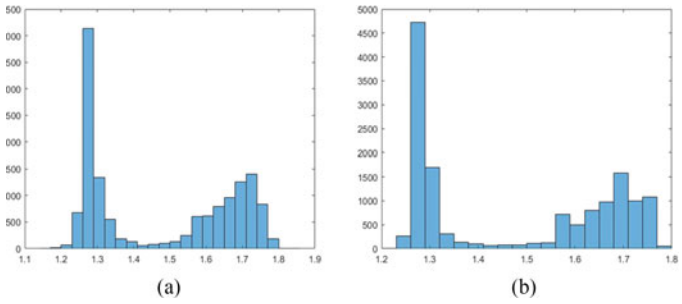

Fig. 7. The histogram of the (a) depth map and (b) recovered depth.

The prediction matrix Q is a function of the depth term and the polarization term of the AR coefficient $a_{x,y}$

$$Q = f(a^{\hat{D}}_{x,y}, a^{I}_{x,y}) = \frac{a^{\hat{D}}_{x,y} a^{I}_{x,y}}{\sum a^{\hat{D}}_{x,y} a^{I}_{x,y}} \tag{16}$$

The unconstrained quadratic nature in (15) is convex, and its global minima is obtained by solving the first order conditions:

$$\underbrace{P^T P + \lambda (I - Q)^T (I - Q)}_{H} d = \frac{P^T d^P}{C} \tag{17}$$

Then, our model for the depth recovery is given by:

$$d = \underbrace{P^T P + \lambda (I - Q)^T (I - Q)}_{H} \setminus \frac{P^T d^P}{C} \tag{18}$$

where H is a squared matrix that is considered the major factor in achieving the stability of the depth recovery model, $\setminus$ is matrix left division used to solve systems of linear equations, and C is equivalent to the d^0 in (8). In the linear equation of first-order conditions, the coefficient matrix is the combination of the sampling matrix P, the prediction matrix Q, and their transposes. Note that $P^T P$ and $(I - Q)^T (I - Q)$ is a highly deficient diagonal matrix. The output of solving this linear equation gives us the recovered depth map.

After applying our proposed method, we recover the estimated depth map. The histogram of the estimated depth D_0 and the recovered depth are shown in Fig. 7.

From Fig. 7, we noticed that the depth values for closer object of our recovered depth map has a higher pixel's number than that of the estimated depth map, and has a lower number for the distant object. This means that our proposed method has overcome the misrepresentation problem of the polarization dehazing.

In Fig. 8(b), it shows the effectiveness in overcoming the problem of the Instant Dehazing method. The red circles show the correction of the depth values corresponding to the same regions in Fig. 7(a). The errors caused by high degree of polarization and sun light direction have been corrected as the bright shades become darker.

Finally, we evaluate our proposed method and show the effectiveness of our proposed method by comparing with the dark channel method [47] and the adaptive AR color-guided (ADAR) model. The experiments and results of different datasets are described in the next section.

4. Experiments and Results

4.1 Data Preparation

In our experiments, we use three datasets of two perpendicular polarized images I_0 and I_{90}: dataset (1) was captured at the old campus (Youyi Road) of Northwestern Polytechnical University (NWPU),

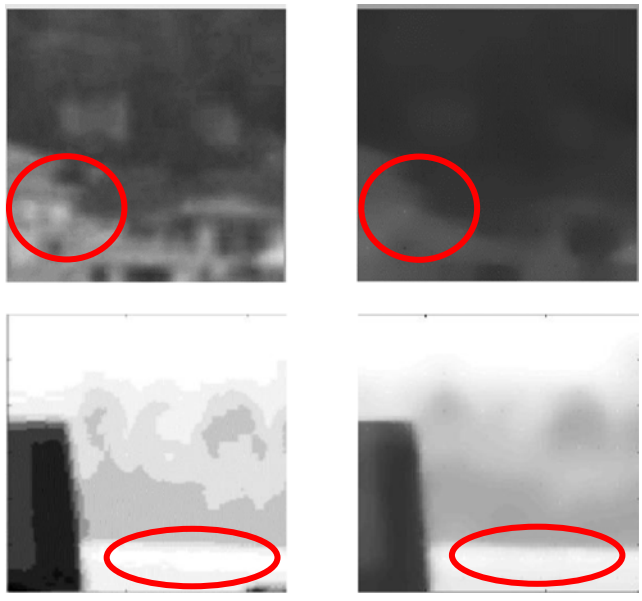

(a) (b)

Fig. 8. The first column (a) the estimated depth map from the polarization method, the second column (b) the recovered estimated depth map by applying our proposed method. (a) Polarization method (b) Proposed method.

Xi'An, China. This data was captured on December 20,2016 at 1:10pm by using iPhone 6s plus (12 Mega pixels) with a polarizing filter. We choose this data to represent an urban environment with buildings at the front of the scene. The scene has very heavy dense haze with max. dark channel $= 235$. The intensity of the dark channel is a rough approximation of the thickness of the haze. A high intensity of the dark channel represents denser haze in the scene.

Datasets (2) and (3) were captured at the new campus of NWPU, in Chang'An region. This data was captured by a Nikon camera D90 (12.3 Mega pixels) with a polarizing filter. Dataset (2) was captured on November 2, 2015 at 2:24pm. It represents a scene of buildings in the front and mountain as the background. The scene has heavy dense haze with max. dark channel=218. Dataset (3) was captured on October 29, 2015 at 3:01pm. This data was chosen to represent a scene of distant buildings and mountain. The scene has dense haze with max. dark channel=176.

We performed image registration for the two-polarized images by the model based on maximization of mutual information [48]. Accurate registration is important to avoid missing aliment between the two-polarized images, which could cause significant error in our experiments.

To dehaze the image by the Instant Dehazing method, we need to estimate the global parameters (the airlight and degree of polarization) at infinite distance. This is done by choosing the pixels at infinite distance, where the brightest pixels in the hazy image are the most haze-opaque. There are two outputs of this method: a dehazed image and an estimated depth.

The estimated depth is used to build our data needed for our method. We compute the S_0 and S_1 from the two perpendicular polarized images I_0 and I_{90}. Then, we tune the AR weight parameters (λ, σ_1, σ_2, σ_3, and σ_4) vital for depth recovery. λ is the parameter that adjusts the importance of the data term and the AR term. σ_1 is the decay rate of the range filter in the depth term that controls the tolerance for two different depth values to be considered close enough to assign a significant weight. σ_2 plays the most important role of the color term, as it controls the decay rate of the exponential function. And σ_3 and σ_4 are the parameters of the bilateral filter to adjust the importance of the spatial distance and intensity difference. Empirically, the model is stable when the parameters are within these following ranges: $\lambda \in [0.01, 0.10]$, $\sigma_1 \in [3.0, 7.0]$, $\sigma_2 \in [3.8, 19.0]$, $\sigma_3 \in [3, 10]$, $\sigma_4 \in [0.01, 0.45]$ [29], [30]. In our experiments, the parameters in the AR model are: $\lambda = 0.01$,

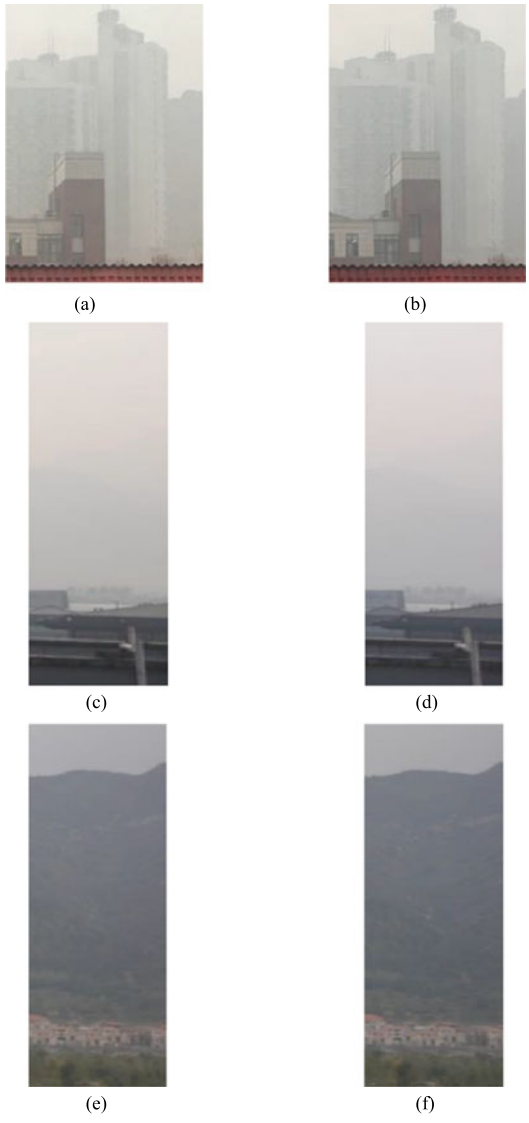

Fig. 9. The three datasets consist of two registered polarized images I_0 and I_{90}. (a) and (b) represent dataset (1) captured in the old campus of NWPU, (c) and (d) represent dataset (2) and (e) and (f) represent data set (3). Both Datasets (2) and (3) are captured in the new campus of NWPU. (a) IMG_r3800 (I_0); (b) IMG_r3829 (I_{90}); (c) DSC_244(I_0); (d) DSC_246(I_{90}); (e) DSC_135 (I_0); (f) DSC_137 (I_{90}).

$\sigma_1 = 4$, $\sigma_2 = 6.67$, $\sigma_3 = 3$, $\sigma_4 = 0.1$. We used size of 120 $\times$ 120 pixels. All the simulation is done using MATLAB R2016a on a laptop I7-6700HQ CPU @ 2.6 GHz, 16 GB RAM, 4 GB NIVIDIA GTX-960M. The computational time of our proposed method for each experiment will be mentioned in the next section.

4.2 Experiments on Datasets

Each of the three dataset is taken from a different environment with different scene contents and has a different haze percentage. The flowchart of the proposed scheme shown in Fig. 2 consists of the following steps:

First, our input is two registered perpendicular polarized images (I_0 and I_{90}).

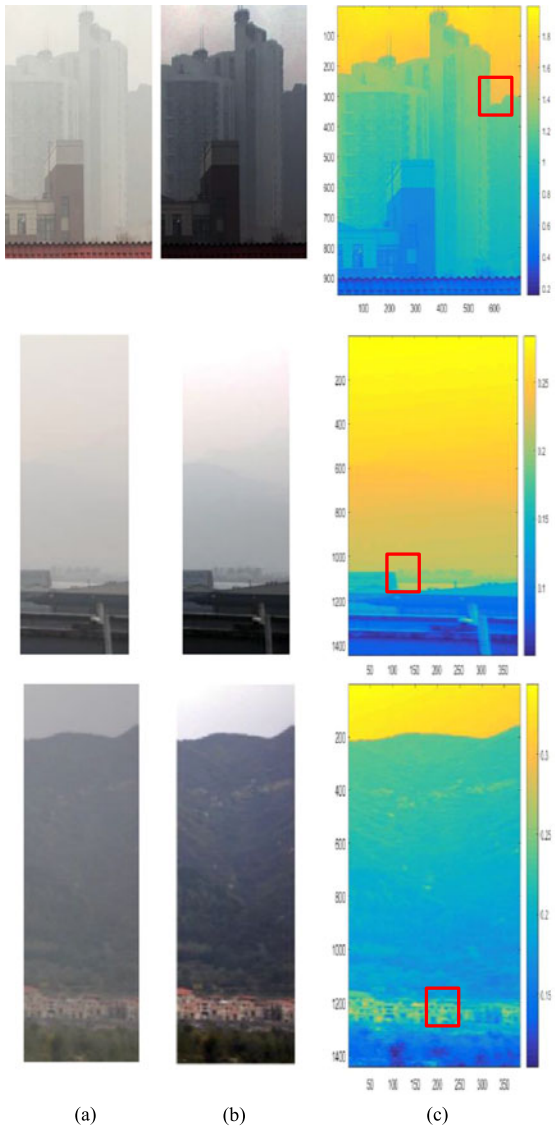

Fig. 10. The haze removal and the estimated depth. The first column (a) is the haze image, the second column (b) is the dehazed image and the third column (c) is depth estimation. The first row is dataset (1), the second row dataset (2) and the third row dataset (3). The red square in the third column (c) represents the magnified region used for further analysis and the colorbar illustrates the depth values. (a) Haze (b) Dehazed (c) Estimated depth.

Second, Instant Dehazing is applied and the output is a dehazed image and an estimated depth map.

Third, we build our datasets which contains the estimated depth map, the polarized images and the Stokes vector components S_0 and S_1.

Fourth, apply our proposed method using the 90-degree polarized image and the Stokes vector component S_1 to get the recovered depth map.

Finally, we evaluate our proposed method by comparing it with the depth obtained from the dark channel method and the ADAR model.

The first three steps of the above- mentioned procedure is to build our datasets. The fourth and fifth steps are to get and evaluate the recovered depth by our proposed method.

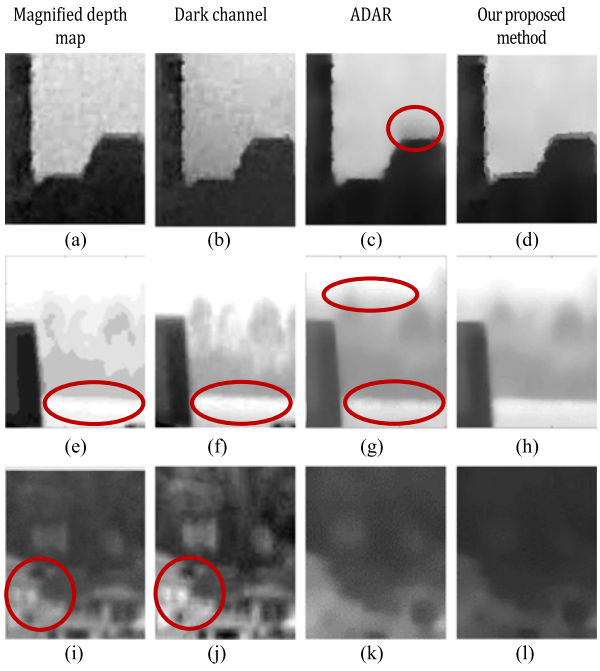

Fig. 11. The depth recovery of the estimated depth map. The first row is the dataset (1), the 2nd dataset (2), the 3rd dataset (3). The first column is the magnified region showed by the red square in the estimated depth map at Fig. 10(c), the second column is the depth from the dark channel method, the third column is the depth recovery by adaptive AR color-guided model and the fourth column is our proposed method.

4.2.1 Registered Polarized Datasets: The three datasets are shown in Fig. 9, each dataset consists of two registered polarized images I_0 and I_{90}.

4.2.2 Haze Removal and Depth Estimation: The outputs of the Instant Dehazing method is shown in Fig. 10. The second column (b) is the dehazed image, while the third column (c) is depth estimation. We selected a region marked by a red square in each dataset. This region with a size of 120×120 is used in our simulation. The closer objects will have a lower value, while distant objects will have a higher value. Some surfaces of closer objects are wrongly estimated as distant ones due to high degree of polarization and the illumination effect of the sun light on building geometry. The degree of polarization of the distant, hazy objects is small relative to the airlight. For closer objects, however, this may not be true. In fact, a significant partial polarization was observed in some surfaces on the closer buildings, especially those directly lit by the sun, which is a problem for the Instant Dehazing method.

4.2.3 Depth Recovery and Evaluation Results: In addition to overcome the problem of the Instant Dehazing method, we notice from Fig. 11 that applying the 90- degree polarization image with the S_1 Stokes vector component has a better result than the dark channel and the ADAR. The dark channel prior is based on the statistics of outdoor haze-free images. It combines the prior with the haze imaging model to obtain a simpler and more effective single dehaze image. The dark channel may not work when the scene objects are inherently similar to the airlight and no shadow is cast on them. As a result, this method will underestimate the transmission of these objects and overestimate the haze layer and could not overcome the depth misrepresentation problem. The ADAR method achieves high quality depth recovery from low quality versions with various degraded depth capturing systems such as ToF cameras and Kinect. While the use of depth cameras is limited by the low quality of produced depth maps, e.g., low resolution, noise, and depth missing in some areas, and it could not overcome the problems of our estimated depth map.

The dataset (1) showed the effectiveness of our proposed method as shown in Fig. 11(d). The edges are more sharp and the depth values are more accurate. The depth from the dark channel method is blurred as shown in Fig. 11(b). The recovered depth of the ADAR in Fig. 11(c) has holes and the edges are blurred, which means the recovered depth is not accurate.

For the dataset (2), some surfaces of closer objects in are wrongly estimated as distant ones (Fig. 11(e)). Those bright shades marked by the red circle shows the errors due to high degree of polarization and the effect of sun illumination. We notice from Fig. 11(f) and (g) that dark channel method and ADAR model have corrected some errors, but still has erroneous holes (marked by the red circles), which means that there is a missing depth value in the recovered depth. On the other hand, in Fig. 11(h), it shows that the edges are more sharp, the bright shades are more dark and without holes, and the depth values are more accurate.

The third row represents the dataset (3). The estimated depth map in Fig. 11(i) has a problem where the values were wrongly estimated as marked by the red circle. The dark channel depth still have the same problem as shown in Fig. 11(j). The output of the ADAR model was shown in Fig. 11(k). The bright shades are more dark but the the edges are blur. On the contrary, our proposed method has sharper edges and more correct depth recovery (Fig. 11(l)).

The computational time of our proposed method by applying it on the estimated depth map was in range of 48$\sim$50 sec. For dataset (1), it was 48.9232 sec as compared to 87.987 sec for the dark channel and 49.5727sec for the ADAR method. For dataset (2), it was 48.7660 sec as compared to 89.432 sec for the dark channel and 49.2127 sec for the ADAR method. For dataset (3), it was 49.8685 sec as compared to 90.5158 sec for the dark channel and 50.0063 sec for the ADAR method. This means that our proposed method has the speed advantage over the dark channel and the ADAR methods and can be described as close to “Instant”.

5. Conclusion

We have proposed a polarization guided auto-regressive model for depth recovery, which is a new method of depth recovery for the estimated depth by polarized images based on AR Model. Our contribution is the polarization guided depth map obtained by applying the Stokes vector component S_1 to the estimated depth guided map obtained from Instant Dehaze method. S_1 gives us the information about the surface of objects and their edges, it also has the Gaussian characteristics that make smoothing effect for reducing noise and to ensure the robustness of our model.

In this paper, we used the Instant Dehazing to get the dehazed image and the estimated depth map. Our experimental results show that using the polarized image I_{90} and the Stokes vector component S_1 give better result as compared to the dark channel method and the adaptive AR color-guided (ADAR) model.

Qualitative evaluation shows the effectiveness and superiority of our proposed method. It also overcomes the problem of the Instant Dehazing method, which misrepresents closer objects as distant objects due to the high degree of polarization and the effect of sun illumination.

Finally, the 90-degree polarized image with the Stokes vector component S_1 outperforms existing the state-of-the-art depth recovery and dehazing method in all datasets, and shows great potential in solving the problem of depth recovery for dehazed polarized images.

Acknowledgment

The authors would like to thank the anonymous reviewers for the associated editor their valuable suggestions.

References

[1] K. Tan and J. P. Oakley, “Enhancement of color images in poor visibility conditions,” in *Proc. 2000 Int. Conf. Image Process.*, 2000, vol. 2, pp. 788–791.

[2] J. P. Oakley and B. L. Satherley, "Improving image quality in poor visibility conditions using a physical model for contrast degradation," *IEEE Trans. Image Process.*, vol. 7, no. 2, pp. 167–179, Feb. 1998.
[3] N. S. Kopeika, *A System Engineering Approach to Imaging*, vol. 3. Bellingham, WA, USA: SPIE, 1998, pp. 277–282.
[4] L. L. Grewe and R. R. Brooks, "Atmospheric attenuation reduction through multisensor fusion," *Proc. SPIE*, vol. 3376, pp. 102–109, 1998.
[5] S. K. Nayar and S. G. Narasimhan, "Vision in bad weather," in *Proc. 7th IEEE Int. Conf. Comput. Vis.*, 1999, pp. 820–827, vol. 2.
[6] S. G. Narasimhan and S. K. Nayar, "Removing weather effects from monochrome images," in *Proc. 2001 IEEE Comput. Soc. Conf. Comput. Vis. Pattern Recognit.*, 2001, vol. 2, pp. II-186–II-193.
[7] F. Cozman and E. Krotkov, "Depth from scattering," in *Proc. IEEE Comput. Soc. Conf. Comput. Vis. Pattern Recognit.*, 1997, pp. 801–806.
[8] D. K. Lynch, "Step brightness changes of distant mountain ridges and their perception," *Appl. Opt.*, vol. 30, pp. 3508–3513, 1991.
[9] S. D. Gedzelman, "Atmospheric optics in art," *Appl. Opt.*, vol. 30, pp. 3514–3522, 1991.
[10] B. T. Sweet and C. L. Tiana, "Image processing and fusion for landing guidance," *Proc. SPIE*, vol. 2736, pp. 84–95, 1996.
[11] P. S. Pencikowski, "Low-cost vehicle-mounted enhanced vision system comprised of a laser illuminator and range-gated camera," *Proc. SPIE*, vol. 2736, pp. 222–227, 1996.
[12] D. Scharstein and R. Szeliski, "A taxonomy and evaluation of dense two-frame stereo correspondence algorithms," in *Proc. IEEE Workshop Stereo and Multi-Baseline Vis.*, 2002, pp. 131–140.
[13] P. Thanusutiyabhorn, P. Kanongchaiyos, and W. S. Mohammed, "Image-based 3D laser scanner," in *Proc. Int. Conf. Elect. Eng./Electron., Comput., Telecommun. Inf. Technol.*, 2011, pp. 975–978.
[14] A. Kolb, E. Barth, R. Koch, and R. Larsen, "Time-of-flight cameras in computer graphics," *Comput. Graph. Forum*, vol. 29, pp. 141–159, 2010.
[15] X. Ye, J. Yang, H. Huang, and C. Hou, "Computational multi-view imaging with kinect," *IEEE Trans. Broadcast.*, vol. 60, no. 3, pp. 540–554, Sep. 2014.
[16] Y. Y. Schechner, S. G. Narasimhan, and S. K. Nayar, "Instant dehazing of images using polarization," in *Proc. 2001 IEEE Comput. Soc. Conf. Comput. Vis. Pattern Recognit.,* 2001, vol. 1, pp. I-325–I-332.
[17] Y. Y. Schechner, S. G. Narasimhan, and S. K. Nayar, "Polarization-based vision through haze," *Appl. Opt.*, vol. 42, pp. 511–525, 2003.
[18] L. B. Wolff, "Polarization vision: A new sensory approach to image understanding," *Image Vis. Comput.*, vol. 15, pp. 81–93, 1997.
[19] R. M. A. Azzam, N. M. Bashara, and S. S. Ballard, "Ellipsometry and polarized light," *Phys. Today,* vol. 31, pp. 270–271, 1978.
[20] M. S. Quinbyhunt, L. L. Erskine, and A. J. Hunt, "Polarized light scattering by aerosols in the marine atmospheric boundarylayer," *Appl. Opt.*, vol. 36, pp. 5168–5184, 1997.
[21] R. MJ *et al.*, "Light backscattering polarization patterns from turbid media: Theory and experiment," *Appl. Opt.*, vol. 38, pp. 3399–3408, 1999.
[22] J. G. Walker, P. C. Chang, and K. I. Hopcraft, "Visibility depth improvement in active polarization imaging in scattering media," *Appl. Opt.*, vol. 39, pp. 4933–4941, 2000.
[23] C. H. Yeh, L. W. Kang, M. S. Lee, and C. Y. Lin, "Haze effect removal from image via haze density estimation in optical model," *Opt. Exp.*, vol. 21, pp. 27127–27141, 2013.
[24] R. L. Lee, "Digital imaging of clear-sky polarization," *Appl. Opt.*, vol. 37, pp. 1465–1476, 1998.
[25] J. E. Solomon, "Polarization imaging," *Appl. Opt.*, vol. 20, pp. 1537–1544, 1981.
[26] A. K. Riemens, O. P. Gangwal, B. Barenbrug, and R. P. M. Berretty, "Multistep joint bilateral depth upsampling," *Proc. SPIE*, vol. 7257, 2009, Art. no. 72570M.
[27] S. A. Guomundsson, R. Larsen, H. Aanaes, and M. Pardas, "TOF imaging in Smart room environments towards improved people tracking," in *Proc. IEEE Comput. Soc. Conf. Comput. Vis. Pattern Recognit. Workshops*, 2008, pp. 1–6.
[28] M. Lindner, A. Kolb, and K. Hartmann, "Data-fusion of PMD-based distance-information and high-resolution RGB-images," in *Proc. Int. Symp. Signals, Circuits Syst.*, 2007, pp. 1–4.
[29] J. Yang, X. Ye, K. Li, and C. Hou, "Depth recovery using an adaptive color-guided auto-regressive model," in *Proc. Eur. Conf. Comput. Vis.*, 2012, pp. 158–171.
[30] J. Yang, X. Ye, K. Li, C. Hou, and Y. Wang, "Color-guided depth recovery from RGB-D data using an adaptive autoregressive model," *IEEE Trans. Image Process.*, vol. 23, no. 8, pp. 3443–3458, Aug. 2014.
[31] Y. Zhao, C. Yi, S. G. Kong, Q. Pan, and Y. Cheng, "Multi-band Polarization Imaging," *J. Sens.*, vol. 2016, pp. 1–10, 2015.
[32] D. Ziou, S. Tabbone, and D. Ziou, "Edge detection techniques - An overview," *Int. J. Pattern Recognit. Image Analysis*, vol. 8, pp. 537–559, 1998.
[33] J. Diebel and S. Thrun, "An application of Markov random fields to range sensing," in *Proc. Int. Conf. Adv. Neural Inf. Process. Syst.*, 2005, pp. 291–298.
[34] B. Huhle, T. Schairer, P. Jenke, and W. Straßer, "Fusion of range and color images for denoising and resolution enhancement with a non-local filter," *Comput. Vis. Image Understanding*, vol. 114, pp. 1336–1345, 2010.
[35] J. Dolson, J. Baek, C. Plagemann, and S. Thrun, "Upsampling range data in dynamic environments," in *Proc. IEEE Conf. Comput. Vis. Pattern Recognit.*, 2010, pp. 1141–1148.
[36] Q. Yang, R. Yang, J. Davis, and D. Nister, "Spatial-depth super resolution for range images," in *Proc. IEEE Conf. Comput. Vis. Pattern Recognit.*, 2007, pp. 1–8.
[37] K. Yemelyanov, M. Lo, P. E., Jr, and N. Engheta, "Display of polarization information by coherently moving dots," *Opt. Exp.*, vol. 11, pp. 1577–1584, 2003.

[38] K. M. Yemelyanov, M. A. Lo, E. N. P., Jr, and N. Engheta, "Display of polarization information by coherently moving dots," *Opt. Exp.*, vol. 11, pp. 1577–1584, 2003.
[39] S. S. Lin, K. M. Yemelyanov, P. E., Jr, and N. Engheta, "Separation and contrast enhancement of overlapping cast shadow components using polarization," *Opt. Exp.*, vol. 14, pp. 7099–7108, 2006.
[40] S. Tominaga and A. Kimachi, "Polarization imaging for material classification," *Opt. Eng.*, vol. 47, pp. 760–760, 2008.
[41] S. S. Lin, K. M. Yemelyanov, P. E., Jr, and N. Engheta, "Separation and contrast enhancement of overlapping cast shadow components using polarization," *Opt. Exp.*, vol. 14, pp. 7099–7108, 2006.
[42] Y. Zhao, *Multi-band Polarization Imaging and Applications*: Berlin, Germany: Springer, 2016.
[43] Y. Zhao, L. Zhang, D. Zhang, and Q. Pan, "Object separation by polarimetric and spectral imagery fusion," *Comput. Vis. Image Understanding*, vol. 113, pp. 855–866, 2009.
[44] Y. Q. Zhao, Q. Pan, Y. C. Chen, and H. C. Zhang, "Clutter reduction based on polarization imaging technology and image fusion theory," *Acta Electronica Sinica*, vol. 33, pp. 433–435, 2005.
[45] M. Bass, *Devices, Measurements, and Properties*, vol. 2. New York, NY, USA: McGraw-Hill, 1995, ch. 22.
[46] S. Fang, X. Xia, H. Xing, and C. Chen, "Image dehazing using polarization effects of objects and airlight," *Opt. Exp.*, vol. 22, pp. 19523–19537, 2014.
[47] K. He, J. Sun, and X. Tang, "Single image haze removal using dark channel prior," in *Proc. IEEE Conf. Comput. Vis. Pattern Recognit.*, 2011, pp. 1956–1963.
[48] F. Maes, A. Collignon, D. Vandermeulen, G. Marchal, and P. Suetens, "Multimodality image registration by maximization of mutual information," *IEEE Trans. Med. Imag.*, vol. 16, no. 2, pp. 187–198, Apr. 1997.